



저작자표시-비영리-변경금지 2.0 대한민국

이용자는 아래의 조건을 따르는 경우에 한하여 자유롭게

- 이 저작물을 복제, 배포, 전송, 전시, 공연 및 방송할 수 있습니다.

다음과 같은 조건을 따라야 합니다:



저작자표시. 귀하는 원저작자를 표시하여야 합니다.



비영리. 귀하는 이 저작물을 영리 목적으로 이용할 수 없습니다.



변경금지. 귀하는 이 저작물을 개작, 변형 또는 가공할 수 없습니다.

- 귀하는, 이 저작물의 재이용이나 배포의 경우, 이 저작물에 적용된 이용허락조건을 명확하게 나타내어야 합니다.
- 저작권자로부터 별도의 허가를 받으면 이러한 조건들은 적용되지 않습니다.

저작권법에 따른 이용자의 권리는 위의 내용에 의하여 영향을 받지 않습니다.

이것은 [이용허락규약\(Legal Code\)](#)을 이해하기 쉽게 요약한 것입니다.

[Disclaimer](#)

**Master of Science**

**Bayesian Uncertainty Quantification of Transition SST Model  
on Flat Plate Transition Flow**

**The Graduate School of**

**University of Ulsan**

**Department of Mechanical Engineering**

**Jae-Hyeon Bae**

**Bayesian Uncertainty Quantification of Transition SST Model  
on Flat Plate Transition Flow**

**Academic advisor: Professor Kyongsik Chang**

**A Thesis**

**Submitted to**

**the Graduate School of University of Ulsan**

**In partial Fulfillment of the Requirements**

**for the Degree of**

**Master of Science**

**by**

**Jae-Hyeon Bae**

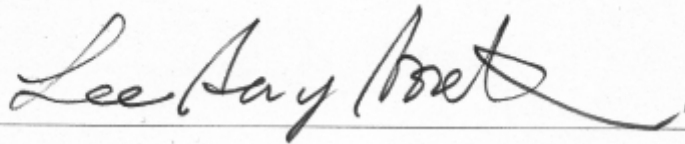
**Department of Mechanical Engineering**

**University of Ulsan, Republic of Korea**

**February 2021**

# **Bayesian Uncertainty Quantification of Transition SST Model on Flat Plate Transition Flow**

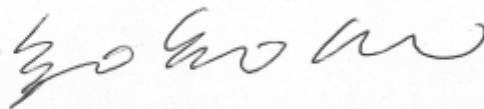
**This certifies that the master thesis of Jae-Hyeon Bae is approved.**



**Committee Chairman Prof. Sang-Wook Lee**



**Committee Member Prof. Jichul Shin**



**Committee Member Dr. Kyoungsik Chang**

**Department of Mechanical Engineering**

**University of Ulsan, Republic of Korea**

**February 2021**

## Abstract

### Bayesian Uncertainty Quantification of Transition SST Model on Flat Plate Transition Flow

Computational study was performed to improve the prediction of transition flow simulated with the Transition SST model. Bayesian inference was applied to calibrated and quantify the uncertainties caused by the Transition SST model coefficients, model inadequacy, and observation error using experiment data. A surrogate model based on the non-intrusive polynomial chaos (NIPC) expansion for effective posterior sampling procedure was applied to predict the skin friction coefficients ( $C_f$ ) for various coefficients of the transition SST model. Variation of transition SST model coefficients was assumed to be independent uniform distributions. Model inadequacy was modeled by a correlated additive Gaussian model with Gaussian covariance function; from the model evidence, Gaussian covariance function was more suitable than the other two covariance function (Linear, Matérn 5/2). Observation error was modeled with an independent additive Gaussian model. The affine invariant ensemble sampler (AIES) algorithm was used to sample the posterior distribution in 2,000 steps and 300 parallel chains. Posterior results showed that uncertainty due to the model inadequacy was greater in predicting  $C_f$  than due to observation error. Prediction of  $C_f$  in transition region was improved by 6% .

**Keywords:** Transition SST model, Uncertainty Quantification (UQ), Non-Intrusive Polynomial Chaos (NIPC), Additive Gaussian Model, Covariance Function, Bayesian Inference, Experiment Data, Monte Carlo Markov Chain (MCMC), Affine invariant ensemble algorithm sampler (AIES), Posterior Distribution

# Contents

Contents .....	i
List of Figures .....	iii
List of Tables .....	iv
Abbreviations .....	v
Chapter 1. Introduction.....	6
Chapter 2. Numerical Methods.....	9
2.1 Governing Equation.....	9
2.2 Transition SST k- $\omega$ .....	10
Chapter 3. Deterministic Simulations .....	15
3.1 Geometry.....	15
3.2 Boundary Conditions .....	15
3.3 Freestream Turbulence decay.....	16
3.4 Grid Test.....	17
Chapter 4. Theoretical Background for UQ .....	19
4.1 The Classification of Uncertainty and UQ.....	19
4.2 Bayesian Inference.....	20
4.3 Non-Intrusive Polynomial Chaos (NIPC).....	20
Chapter 5. Bayesian Inference for the Flat Plate Transition Flow.....	23
5.1 Stochastic Model .....	23
5.1.1 Parameter Uncertainty .....	23
5.1.2 Model Inadequacy .....	25
5.1.3 Observation Error.....	27

5.2 Likelihood Function.....	28
5.3 Markov Chain Monte Carlo (MCMC).....	29
5.4 Posterior Distribution.....	30
5.4.1 Model Evidence .....	30
5.4.2 Posterior Results.....	31
Chapter 6. Conclusion .....	39
REFERENCE.....	40

## List of Figures

<b>Figure 1.</b> Computational domain .....	15
<b>Figure 2.</b> Boundary conditions .....	16
<b>Figure 3.</b> Turbulence decay along the flat plate .....	17
<b>Figure 4.</b> $C_f$ along the flat plate depending on grid size.....	18
<b>Figure 5.</b> Validation error according to the 16 monitoring points.....	25
<b>Figure 6.</b> Correlation metrics for each covariance function.....	27
<b>Figure 7.</b> Posterior distribution for $\pm 10\%$ interval $c_{a1}$ .....	32
<b>Figure 8.</b> Posterior distribution for $\pm 10\%$ interval $c_{e1}$ .....	32
<b>Figure 9.</b> Posterior distribution for $\pm 10\%$ interval $c_{a2}$ .....	32
<b>Figure 10.</b> Posterior distribution for $\pm 10\%$ interval $c_{e2}$ .....	32
<b>Figure 11.</b> Posterior distribution for $\pm 50\%$ interval $c_{a1}$ .....	34
<b>Figure 12.</b> Posterior distribution for $\pm 50\%$ interval $c_{e1}$ .....	34
<b>Figure 13.</b> Posterior distribution for $\pm 50\%$ interval $c_{a2}$ .....	34
<b>Figure 14.</b> Posterior distribution for $\pm 50\%$ interval $c_{e2}$ .....	34
<b>Figure 15.</b> Posterior distribution for $\pm 50\%$ interval $\sigma_\gamma$ .....	35
<b>Figure 16.</b> Posterior distribution for $\pm 50\%$ interval $c_{\theta t}$ .....	35
<b>Figure 17.</b> Posterior distribution for $\pm 50\%$ interval $\sigma_{\theta t}$ .....	35
<b>Figure 18.</b> Posterior distribution for $\pm 50\%$ interval $\sigma_\eta$ .....	36
<b>Figure 19.</b> Posterior distribution for $\pm 50\%$ interval $\sigma_e$ .....	36
<b>Figure 20.</b> $C_f$ predictions using calibrated model coefficients .....	38
<b>Figure 21.</b> $C_f$ prediction errors compared with nominal values.....	38



## List of Tables

<b>Table 1.</b> Specific boundary conditions.....	16
<b>Table 2.</b> Grid independence test .....	17
<b>Table 3.</b> List of classic univariate polynomial families .....	22
<b>Table 4.</b> Transition SST model closure coefficients $\pm 50\%$ intervals.....	24
<b>Table 5.</b> Posterior plausibility of the model classes.....	31
<b>Table 6.</b> Calibrated Transition SST model closure coefficients .....	37

## Abbreviations

AIES	Affine Invariant Ensemble Sampling
$C_f$	Skin Friction Coefficient
CFD	Computational Fluid Dynamics
gPC	generalized Polynomial Chaos
HDMR	High-Dimensional Model Representation
MCMC	Markov Chain Monte Carlo
NIPC	Non-Intrusive Polynomial Chaos
QoI	Quantities of Interest
RANS	Reynolds-Averaged Navier-Stokes
SC	Stochastic collocation
SST	Shear Stress Transport
UQ	Uncertainty quantification

## Chapter 1. Introduction

Prediction of transition region is important in many engineering problems. In the turbulent boundary layer, since the motion of the fluid is chaotic and shows 3D unsteady behavior, heat transfer and wall shear stress increase, and the characteristic of separation behavior is improved compared to that of laminar. For this reason, many engineering applications, such as turbo machines and wind turbines, have used the transition turbulence model to predict the transition region. However, predicting a transition region using the Reynolds-averaged Navier-Stokes (RANS) model has limitations because complex transition and turbulence mechanisms are modeled with heuristic and mathematical assumptions. It means that RANS model has the uncertainty caused by model and model coefficients. Boundaries, initial conditions, geometry uncertainties, and discretization errors can also be a source of uncertainty in computational fluid dynamics (CFD) situations.

With the rapid development of computational power, efforts to quantify and reduce uncertainty associated with computational models has attracted much attention. There are two kinds of processes to quantify uncertainty. One is the forward problem, which quantifies the propagation of uncertainty by computational simulation, and the other is the inverse problem, which is the process of quantifying the input random variables and calibrating the model from the observation.

Hosder et al. [1] applied the non-intrusive polynomial chaos (NIPC) expansion based on the spectral representation of the uncertainty to quantify the propagation of input uncertainty in CFD simulations. They simulated (1) the inviscid oblique shock wave problem with geometric uncertainty, (2) the inviscid expansion wave problem with geometric uncertainty, and (3) the subsonic laminar boundary layer flow over a flat plate with a free-stream dynamic viscosity uncertainty to validate the NIPC method. Their NIPC results were in good agreement with Monte Carlo simulations. They also found that a

fourth-order polynomial chaos expansion was sufficient to approximate the statistics and the shape of the output uncertainty distributions with appropriate accuracy.

Schaefer et al. [2] employed uncertainty quantification and sensitivity analysis of turbulent models in RANS codes due to uncertainty in the value of each closure coefficients. Transonic flow over an axisymmetric bump and the RAE 2822 transonic airfoil with three turbulent models (the Spalart-Allmaras model, the Wilcox (2006)  $k-\omega$  model, and the SST  $k-\omega$ ) was simulated. Their uncertainty propagation analysis was conducted by NIPC. Each closure coefficient was ranked by the contribution of uncertainty in integrated and point quantities by Sobol indices. They identified several closure coefficients in each turbulence model, for which more information would significantly reduce the amount of uncertainty in the output for transonic wall-bounded flows.

The previous two studies focused on quantifying the propagation of uncertainty in computational simulations and found the major model coefficients that contributed to the uncertainty. But the following studies applied Bayesian inference for the inverse problem, wherein unknown parameters that cannot be directly measured are estimated based on experimental data.

Cheung et al. [3] applied Bayesian uncertainty quantification techniques to the calibration processes in the Spalart-Allmaras turbulence model. They also suggested three competing model classes and compared them in terms of their posterior probabilities and their prediction of quantities of interest (QoIs). The model posterior probability represents the relative plausibility of each model class given the data. The stochastic model with correlated Gaussian uncertainty is overwhelmingly favored over the other two model classes.

Zhang et al. [4] proposed the Bayesian uncertainty quantification approach using the adaptive high-dimensional model representation (HD MR) technique and the stochastic

collocation (SC) method based on generalized polynomial chaos (gPC) to construct a surrogate model for the sampling procedure in Bayesian calibration. They also conducted a rigorous convergence study of the approximate posterior for the proposed approach using simple mathematical functions and a  $k$ - $\omega$ - $\gamma$  transition model. Their results showed not only that the quantified uncertainty overlapped well with the experimental data, but also a great improvement of the match between the prediction mean and the experimental data.

In the present work, three uncertainty sources were quantified and calibrated by Bayesian inference with the experimental data (T3A) [5]. The Bayesian approach is one general method to treat the inverse problem, where the goal is to back-propagate information about the observation to obtain insight on the input parameters. Here, the uncertainties came from the model coefficients, the model inadequacy, and the observation error. Uncertainty from the model coefficients was modeled with independent uniform distributions within  $\pm 10\%$  and  $\pm 50\%$  intervals from each nominal value because do not know exact range of uncertainty. Simulation results according to the model coefficients were replaced with NIPC expansion-based surrogate model. Because the surrogate model is cheaper than 2D flat plate simulation in a posterior sampling procedure. Uncertainty from the model inadequacy was modeled with a correlated additive Gaussian model with three kinds of covariance functions, and uncertainty from the observation error was modeled with an independent additive Gaussian model. The AIES algorithm was used to sample the posterior distribution in 2,000 steps and 300 parallel chains.

## Chapter 2. Numerical Methods

In this chapter, the numerical method is explained. This work incorporates a Transition SST model to simulate a 2D flat plate transition flow. The fluid is considered incompressible and viscous, and the flow is assumed to be steady-state. The SIMPLE-Consistent (SIMPLEC) algorithm [7] is used for pressure and velocity coupling. All spatial discretization schemes use the second order upwind scheme.

### 2.1 Governing Equations

These assumptions are used here.

1. Incompressible and viscous fluid.
2. The flow is steady-state.
3. The gravity can be neglected.

Considering these assumptions, the mass conservation equation can be expressed as:

$$\frac{\partial u_i}{\partial x_i} = 0 \quad (2.1)$$

where  $\rho$  is the density of the fluid and  $u_i$  are the each velocity components. The momentum conservation equation (called the Navier-Stokes equation) can be written as follows:

$$\frac{\partial u_i}{\partial t} + \frac{\partial (u_i u_j)}{\partial x_j} = -\frac{1}{\rho} \frac{\partial p}{\partial x_i} + \frac{\partial}{\partial x_j} \left( \nu \frac{\partial u_i}{\partial x_j} - \overline{u'_i u'_j} \right) \quad (2.2)$$

where  $-\overline{u'_i u'_j}$  is the Reynolds stress term; how this term is modeled creates the difference between turbulence models (in this case, RANS Transition SST model). These governing equations were discretized with the second-order upwind scheme, and SIMPLEC was used

for the pressure-velocity coupling method.

## 2.2 Transition SST k- $\omega$

The Transition SST k- $\omega$  model was proposed by Menter and Lengry [6]. It is also known as the  $\gamma$ - $Re_\theta$  model or the k- $\omega$  SSTLM. The transition SST k- $\omega$  model includes two additional transport equations to estimate the transition, one for intermittency  $\gamma$  and one for a Reynolds number based on the transition onset momentum thickness,  $\tilde{Re}_{\theta t}$ . The transport equation for the intermittency  $\gamma$  is described as follows:

$$\frac{\partial(\rho\gamma)}{\partial t} + \frac{\partial(\rho U_j \gamma)}{\partial x_j} = P_\gamma - E_\gamma + \frac{\partial}{\partial x_j} \left[ \left( \mu + \frac{\mu_t}{\sigma_\gamma} \right) \frac{\partial \gamma}{\partial x_j} \right] \quad (2.3)$$

The intermittency source term controls the length of the transition region, and the dissipation term allows the boundary layer to relaminarize. Each term is defined as follows:

$$P_\gamma = F_{length} c_{a1} \rho S [\gamma F_{onset}]^{0.5} (1 - c_{e1} \gamma) \quad (2.4)$$

where  $S$  is the strain rate magnitude,  $F_{length}$  controls the strength of the production, and  $F_{onset}$  switches the production of  $\gamma$ .

$$E_\gamma = c_{a2} \rho \Omega \gamma F_{turb} (c_{e2} \gamma - 1) \quad (2.5)$$

where  $\Omega$  is the vorticity magnitude.

If  $F_{length}$  is very large,  $\gamma$  is going to be produced very rapidly and will saturate to a value of 1 very quickly. This results in a short length of the transition region.  $F_{onset}$  is a type of

switch function that has a value of 0 for the laminar region; it is activated as the production term for transition region in the boundary layer.  $F_{length}$  is based on  $\tilde{Re}_{\theta t}$  from an empirical correlation, and  $F_{onset}$  is a function of  $Re_{\theta c}$  as follows:

$$F_{length} = \begin{cases} [398.189 \cdot 10^{-1} + (-119.27 \cdot 10^{-4})\tilde{Re}_{\theta t} + (-132.567 \cdot 10^{-6})\tilde{Re}_{\theta t}^2] & \tilde{Re}_{\theta t} < 400 \\ [263.404 + (-123.939 \cdot 10^{-2})\tilde{Re}_{\theta t} + (194.548 \cdot 10^{-5})\tilde{Re}_{\theta t}^2 + (-101.695 \cdot 10^{-8})\tilde{Re}_{\theta t}^3] & 400 \leq \tilde{Re}_{\theta t} < 596 \\ [0.5 - (\tilde{Re}_{\theta t} - 596.0) \cdot 3.0 \cdot 10^{-4}] & 596 \leq \tilde{Re}_{\theta t} < 1200 \\ [0.3188] & \tilde{Re}_{\theta t} < 1200 \end{cases} \quad (2.6)$$

$$Re_V = \frac{\rho y^2 S}{\mu} \quad (2.7)$$

$$F_{onset1} = \frac{Re_V}{2193 Re_{\theta c}} \quad (2.8)$$

$$F_{onset2} = \min(\max(F_{onset1}, F_{onset1}^4), 2.0) \quad (2.9)$$

$$R_T = \frac{\rho k}{\mu \omega} \quad (2.10)$$

$$F_{onset3} = \max\left(1 - \left(\frac{R_T}{2.5}\right)^3, 0\right) \quad (2.11)$$

$$F_{onset} = \max(F_{onset2} - F_{onset3}, 0) \quad (2.12)$$

where  $y$  is the wall distance and  $Re_{\theta c}$  is Reynolds number based on momentum thickness which turbulent fluctuation onset. The constants for the intermittency equation are:

$$c_{a1} = 2.0; c_{e1} = 1.0; c_{a2} = 0.06; c_{e2} = 50; \sigma_y = 1.0.$$



The transport equation for the transition momentum thickness Reynolds  $\tilde{Re}_{\theta t}$  is:

$$\frac{\partial(\rho\tilde{Re}_{\theta t})}{\partial t} + \frac{\partial}{\partial x_j}(\rho U_j \tilde{Re}_{\theta t}) = P_{\theta t} + \frac{\partial}{\partial x_j} \left[ \sigma_{\theta t} (\mu + \mu_t) \frac{\partial}{\partial x_j} (\tilde{Re}_{\theta t}) \right] \quad (2.13)$$

$$P_{\theta t} = C_{\theta t} \frac{\rho}{t} (Re_{\theta t} - \tilde{Re}_{\theta t})(1.0 - F_{\theta t}) \quad (2.14)$$

$$t = \frac{500\mu}{\rho U^2} \quad (2.15)$$

Outside the boundary layer, the source term is included to force  $\tilde{Re}_{\theta t}$  to take the local value of  $Re_{\theta t}$  calculated from the empirical correlation. In Eq. (2.14), the blending function  $F_{\theta t}$  makes the source turn off in the boundary layer and allows the transported scalar  $\tilde{Re}_{\theta t}$  to diffuse from the freestream.  $F_{\theta t}$  is equal to 0 in the freestream and is 1 near the wall.

$$F_{\theta t} = \min \left[ \max \left\{ F_{wake} e^{(-\frac{y}{\delta})^4}, 1.0 - \left( \frac{\gamma - 1/c_{e2}}{1.0 - 1/c_{e2}} \right)^2 \right\}, 1.0 \right] \quad (2.16)$$

$$\theta_{BL} = \frac{\tilde{Re}_{\theta t} \mu}{\rho U}, \delta_{BL} = \frac{15}{2} \theta_{BL}, \delta = \frac{50\Omega y}{U} \delta_{BL}, Re_{\omega} = \frac{\rho \omega y^2}{\mu} \quad (2.17)$$

$$F_{wake} = e^{-\left(\frac{Re_{\omega}}{1E5}\right)^2} \quad (2.18)$$

The boundary condition for  $\tilde{Re}_{\theta t}$  at a wall is zero flux. The boundary condition for  $\tilde{Re}_{\theta t}$  at an inlet should be calculated from the empirical correlation in Eq. (2.21) based on

the inlet turbulence intensity as follows:

$$Tu = \frac{100}{U} \sqrt{\frac{2}{3}k} \quad (2.19)$$

$$\lambda_\theta = \frac{\rho\theta^2}{\mu} \cdot \frac{dU}{ds}, \quad \frac{dU}{ds} = \left[ (u/U) \frac{dU}{dx} + (v/U) \frac{dU}{dy} + (w/U) \frac{dU}{dz} \right] \quad (2.20)$$

$$Re_{\theta t} = \begin{cases} \left[ 1173.51 - 589.428Tu + \frac{0.2196}{Tu^2} \right] F(\lambda_\theta) & Tu \leq 1.3 \\ 331.50[Tu - 0.5658]^{-0.671} F(\lambda_\theta) & Tu > 1.3 \end{cases} \quad (2.21)$$

$$F(\lambda_\theta) = \begin{cases} 1 - [-12.986\lambda_\theta - 123.66\lambda_\theta^2 - 405.689\lambda_\theta^3] e^{-\left(\frac{Tu}{1.5}\right)^{1.5}} & \lambda_\theta \leq 0 \\ 1 + 0.275[1 - e^{-35.0\lambda_\theta}] e^{\left[\frac{-Tu}{0.5}\right]} & \lambda_\theta > 0 \end{cases} \quad (2.22)$$

For numerical robustness, the acceleration parameters, the turbulence intensity, and the empirical correlation should be limited as follows:

$$-0.1 \leq \lambda_\theta \leq 0.1 \quad Tu \geq 0.027 \quad Re_{\theta t} \geq 20$$

The model constants for the  $\tilde{R}e_{\theta t}$  equations are:  $c_{\theta t} = 0.03$ ;  $\sigma_{\theta t} = 2.0$ .

The transition model interacts with the SST k- $\omega$  as follows:

$$\frac{\partial(\rho k)}{\partial t} + \frac{\partial(\rho U_j k)}{\partial x_j} = \tilde{P}_k - \tilde{D}_k + \frac{\partial}{\partial x_j} \left[ (\mu + \sigma_k \mu_t) \frac{\partial \gamma}{\partial x_j} \right] \quad (2.23)$$

$$\tilde{P}_k = \gamma_{eff} P_k; \quad \tilde{D}_k = \min(\max(\gamma_{eff}, 0.1), 1.0) D_k \quad (2.24)$$

$$R_y = \frac{\rho y \sqrt{k}}{\mu}; \quad F_3 = e^{-\left(\frac{R_y}{120}\right)^8}; \quad F_1 = \max(F_{1orig}, F_3) \quad (2.25)$$

where  $P_k$  and  $D_k$  are the original production and destruction terms of the SST k- $\omega$ , and  $F_{1orig}$  is the blending function for the original SST k- $\omega$ . As shown in Eq. (2.24), the production term is going to zero when  $\gamma$  has the value of zero at the laminar boundary layer, but the production term has the same value as that of SST k- $\omega$  in the turbulent boundary layer.

## Chapter 3. Deterministic Simulations

This chapter shows a deterministic simulation setup to create the dataset used to construct the surrogate model. The boundary conditions were assigned similarly to Coupland's experiment [5]. The inlet turbulence intensity was assigned considering the turbulence decay. A grid convergence test was also conducted.

### 3.1 Geometry

The geometry is adopted from the simulation of Malan et al [8]. The domain extended from 0.15m upstream of the plate to 1.7m. The domain height was 0.3m. Details of the geometry and computational domain are shown in Fig 1.

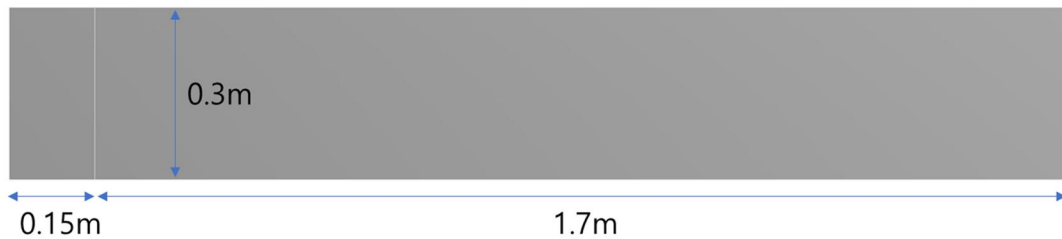
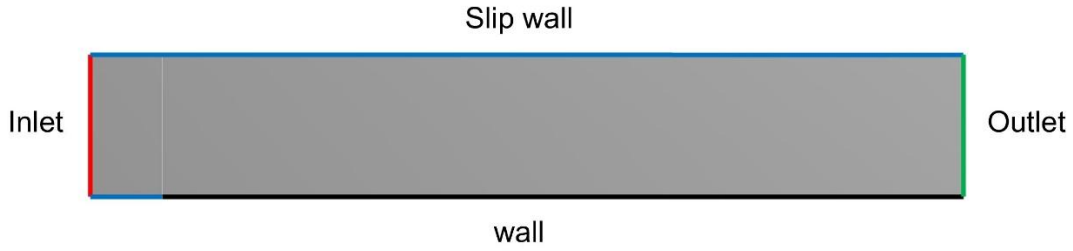


Figure 1. Computational domain

### 3.2 Boundary Conditions

The Reynolds number, which was based on the plate length  $L$  (1.7 m) and the inlet velocity  $U$  (5.4 m/s) was  $6.3 \times 10^5$ . Because of turbulence decay, the turbulence intensity of the inlet was set to 4.0% and the decay was set to the value of Coupland's experiment (3%) at the leading edge. Slip walls were used on the top boundary and upstream of the plate. Fluid density was taken to be  $1.2 \text{ kg/m}^3$  and the viscosity as  $1.8 \text{ kg/m}$ . More details are shown in Fig. 2 and Table 1.



**Figure 2. Boundary conditions**

**Table 1. Specific boundary conditions**

Name	Boundary condition	Value
Inlet	Velocity inlet ( $m/s$ )	$U=5.4$
	Turbulence intensity (%)	$Tu = 4.0$
	Turbulent kinetic energy ( $m^2/s^2$ )	0.06998
	Specific dissipation rate ( $1/s$ )	159.7
Outlet	Pressure outlet	$P = 0Pa$
Slip wall	Slip	$Shear\ stress = 0Pa$
Wall	No slip	-

### 3.3 Freestream Turbulence decay

The turbulence intensity specified at the inlet can decay depending on the inlet viscosity ratio. Therefore, validation of the turbulence intensity is important in the Transition SST model because the turbulence intensity at the leading edge can be smaller than the inlet value. The good agreement with the experimental data shown in Fig. 3 indicates that appropriate boundary conditions (inlet turbulence intensity, turbulent viscosity ratio) were used in this simulation.

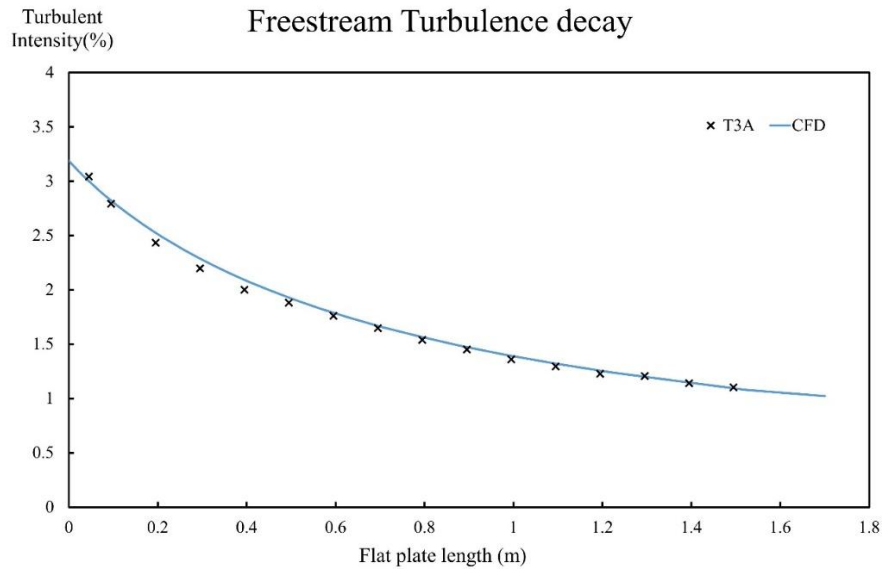


**Figure 3. Turbulence decay along the flat plate**

### 3.4 Grid Test

The grid test was achieved using coarse ( $83 \times 112$  nodes), medium ( $100 \times 135$  nodes), and fine mesh ( $144 \times 194$  nodes), as shown in Table 2. The height of the first cell from the wall was set to  $10^{-5}$  m for resolving the turbulent boundary layer. The skin friction coefficient ( $C_f$ ) was compared along the flat plate length depending on the number of nodes, as shown in Fig. 4. The figure shows that the fine mesh estimated the transition region earlier than the experimental data, but the coarse mesh had the opposite result. The medium mesh showed good agreement with the experimental data. Thus, the medium mesh was selected as appropriate in this work.

**Table 2. Grid independence test**

	Coarse	Medium	Fine
Number of nodes	9,296	13,500	27,936

## Grid Convergence Test

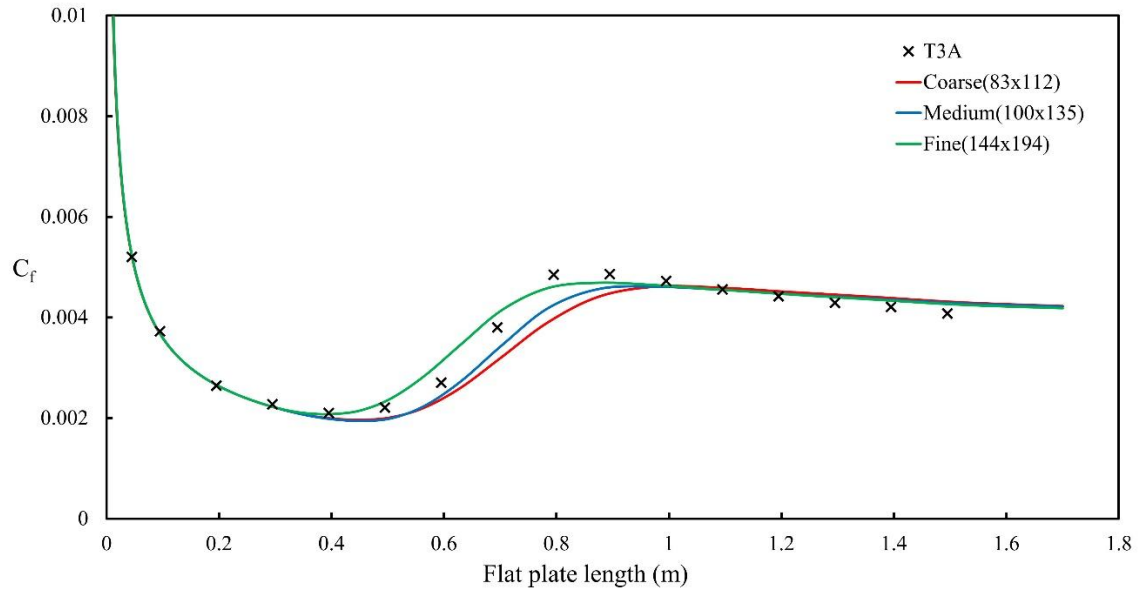


Figure 4.  $C_f$  along the flat plate depending on grid size

## **Chapter 4. Theoretical Background for UQ**

### **4.1 The Classification of Uncertainty and UQ**

Uncertainty is a factor that causes errors in predictions and observations. It can enter computational models and experimental measurements in various contexts. The sources of uncertainty can be categorized as follows [9]:

1. Parameter uncertainty: This comes from the model parameters that are inputs to the computational model (mathematical model) but whose exact values are unknown to the experimentalists and cannot be controlled in physical experiments, or whose values cannot be exactly inferred by statistical methods (e.g., boundaries, initial conditions, model coefficients, etc.)

2. Model inadequacy: This comes from the lack of knowledge of the underlying physics in the problem. It depends on how accurately a mathematical model describes the true system for a real-life situation, considering the fact that models are almost always only approximations of reality (e.g., RANS, Euler equation, etc.)

3. Observation error: This comes from the variability of experimental measurements. The experimental uncertainty is inevitable and can be determined by repeating a measurement many times, using exactly the same settings for all of the inputs/variables.

These uncertainties can be expressed in terms of probability distributions and quantified by “uncertainty quantification” (UQ). UQ is the process of quantifying and reducing the uncertainties in both computational models and observed real-world phenomena. There are two major types of problems in UQ. One is the forward propagation of uncertainty, where the various sources of uncertainty are propagated through the model to predict the overall uncertainty in the system response. The other is the inverse problem of model uncertainty and parameter uncertainty, where the model parameters are calibrated



simultaneously using observation data. The present work focuses on the inverse problem using Bayesian inference to quantify the model inadequacy, observation error, and finally calibrate the model coefficients. The entire process of UQ was here conducted by the UQLab framework [10] using MATLAB [11].

## 4.2 Bayesian Inference

The Bayesian method is a powerful tool to address the inverse problem, where the goal is to back-propagate information about an observation to obtain insight on the model inputs. Bayesian inference can estimate parameters using only a handful of data points, compared with data-heavy statistical inference. In Bayesian inference, the parameters are inferred by combining some prior knowledge on the parameters with the observed data using Bayes' theorem as follows:

$$\pi(\theta|d) = \frac{\pi(d|\theta)\pi(\theta)}{\pi(d)} \quad (4.1)$$

where  $\theta$  are the uncertainty parameters to be inferred and  $\pi(\theta)$  is the prior distribution of the parameters. The choice of prior distribution should reflect the level of information existing on the parameters  $\theta$  before any measurement is carried out.  $\pi(d|\theta)$  is the likelihood (or likelihood function) that represents an estimate of a parameter, and it indicates which parameters are most likely.  $\pi(d)$  is a normalizing factor known as the evidence or marginal likelihood. From these we can estimate the posterior distribution of the parameters.

### 4.3 Non-Intrusive Polynomial Chaos (NIPC)

Deterministic modeling is being gradually replaced by stochastic modeling to account for the inevitable uncertainty in physical phenomena and measurements. It requires modification of the deterministic code, and this may be inconvenient for many complex computational problems since the modification of the existing code can be difficult, expensive, and time-consuming [12]. Metamodeling (or surrogate modeling) attempts to offset the increased costs of stochastic modeling by substituting the expensive-to-evaluate computational models (like CFD) with inexpensive-to-evaluate surrogate model [13]. NIPC expansions are a powerful metamodeling technique that aims at providing a functional approximation of a computational model through its spectral representation on a suitably built basis of polynomial functions.

The method is to define the joint probability density function  $f_{\mathbf{X}}$  from a random vector with independent components  $\mathbf{X} \in \mathbb{R}^M$ . The next step is to consider a finite variance computational model as a map  $Y = \mathcal{M}(\mathbf{X})$ ,  $Y \in \mathbb{R}$  such that:

$$\mathbb{E}[Y^3] = \int_{\mathcal{D}_{\mathbf{X}}} \mathcal{M}^2(\mathbf{X}) f_{\mathbf{X}}(x) dx < \infty \quad (4.2)$$

Then the polynomial chaos expansion of  $\mathcal{M}(\mathbf{X})$  is defined as follows:

$$\mathcal{M}(\mathbf{X}) \approx \mathcal{M}^{PC}(\mathbf{X}) = \sum_{\alpha \in A} y_{\alpha} \psi_{\alpha}(\mathbf{X}) \quad (A \subset \mathbb{N}^M) \quad (4.3)$$

where  $y_{\alpha} \in \mathbb{R}$  are the corresponding coefficients, and  $A \subset \mathbb{N}^M$  is the set of selected multi-indices of multivariate polynomials. In Eq. (4.4), the  $\psi_{\alpha}(\mathbf{X})$  are the multivariate

polynomials that are assembled as the tensor product of their univariate counterparts, shown in Table 3.

$$\psi_\alpha(\mathbf{X}) \equiv \prod_{i=1}^M \phi_{\alpha_i}^{(i)}(x_i) \quad (4.4)$$

**Table 3. List of classic univariate polynomial families**

Type of variable	Distribution	Orthogonal polynomials	Hilbertian basis $\psi_k(x)$
Uniform $U(-1,1)$	$\frac{1(x)}{2}$	Legendre $P_k(x)$	$P_k(x) / \sqrt{\frac{1}{2k+1}}$
Gaussian $G(0,1)$	$\frac{1}{\sqrt{2\pi}} e^{-x^2/2}$	Hermite $H_{e_k}(x)$	$H_{e_k}(x) / \sqrt{k!}$
Gamma $\Gamma(a, \lambda = 1)$	$x^a e^{-x}$	Laguerre $L_k^a(x)$	$L_k^a(x) / \sqrt{\frac{\Gamma(k+a+1)}{k!}}$
Beta $B(a, b)$	$1(x) \frac{(1-x)^a (1+x)^b}{B(a)B(b)}$	Jacobi $J_k^{a,b}(x)$	$J_k^{a,b}(x) / \mathfrak{S}_{a,b,k}$

# Chapter 5. Bayesian Inference for the Flat Plate Transition Flow

## 5.1 Stochastic Model

As mentioned in the previous chapter, three uncertainty sources are considered in the Bayesian inference. Each uncertainty source is modeled in terms of a stochastic model. Uncertainty from the model coefficients is treated as parameter uncertainty and it is modeled with independent uniform distributions within  $\pm 10\%$ ,  $\pm 50\%$  intervals from each nominal value because do not have any information and is calibrated to fit well with experimental data [5] by Bayesian inference. Simulation results according to the model coefficient uncertainty is replaced by the NIPC expansion-based surrogate model for effective posterior sampling. RANS error propagation through the domain was treated as model inadequacy. Model inadequacy was modeled with a correlated additive Gaussian model with three kinds of covariance functions to represent the spatial correlation. Finally, observation error is modeled with an independent additive Gaussian model.

### 5.1.1 Parameter Uncertainty

Model coefficients ensure robustness in common problems and prevent non-physical results, but they can reveal the error in complex or specific problems. Therefore, this work assumes that the model coefficients are treated as parameter uncertainty and will reduce the error through the Bayesian inference based on experimental data [5]. The Transition SST model has seven model coefficients for intermittency  $\gamma$ , and a transition onset momentum thickness Reynolds number  $\tilde{Re}_{\theta t}$ . Because of we do not have any information about the model coefficients uncertainty range, it is modeled with two kinds of range ( $\pm 10\%$  and  $\pm 50\%$  intervals from each nominal value) with independent uniform distributions and proper range can be found by posterior distribution. If range of uncertainty is small, the

most of posterior samples are truncated at the edge of domain.

**Table 4. Transition SST model closure coefficients  $\pm 50\%$  intervals**

Model Coefficient	Nominal Value	Lower Bound	Upper Bound
$c_{a1} \sim \text{Uniform}$	2.0	1.0	3.0
$c_{e1} \sim \text{Uniform}$	1.0	0.5	1.5
$c_{a2} \sim \text{Uniform}$	0.06	0.03	0.09
$c_{e2} \sim \text{Uniform}$	50.0	25.0	75.0
$\sigma_\gamma \sim \text{Uniform}$	1.0	0.5	1.5
$c_{\theta t} \sim \text{Uniform}$	0.03	0.015	0.045
$\sigma_{\theta t} \sim \text{Uniform}$	2.0	1.0	3.0

However, in the posterior sampling procedure of Bayesian inference, it is time-intensive to calculate the CFD results according to the model coefficient variation. Therefore, in order to alleviate this problem, the NIPC-based surrogate model used here was constructed from 200 CFD data points and was used in the posterior sampling procedure that required at least tens of thousands of simulation repetitions.

$$\mathcal{M}(\mathbf{X}) \approx \mathcal{M}^{PC}(\mathbf{X}), \quad \mathbf{X} = [c_{a1}, c_{e1}, c_{a2}, c_{e2}, \sigma_\gamma, c_{\theta t}, \sigma_{\theta t}] \quad (5.1)$$

After constructing a surrogate model, it is necessary to evaluate how accurately it predicts. Therefore, 160 data points were used for the training set and 40 data points were used for the validation set. Validation of the surrogate models was accomplished using the validation error as follows:

$$\epsilon_{val} = \frac{N-1}{N} \left[ \frac{\sum_{i=1}^N \left( \mathcal{M}(\mathbf{X}_{val}^{(i)}) - \mathcal{M}^{PC}(\mathbf{X}_{val}^{(i)}) \right)^2}{\sum_{i=1}^N \left( \mathcal{M}(\mathbf{X}_{val}^{(i)}) - \hat{\mu}_{y_{val}} \right)^2} \right] \quad (5.2)$$

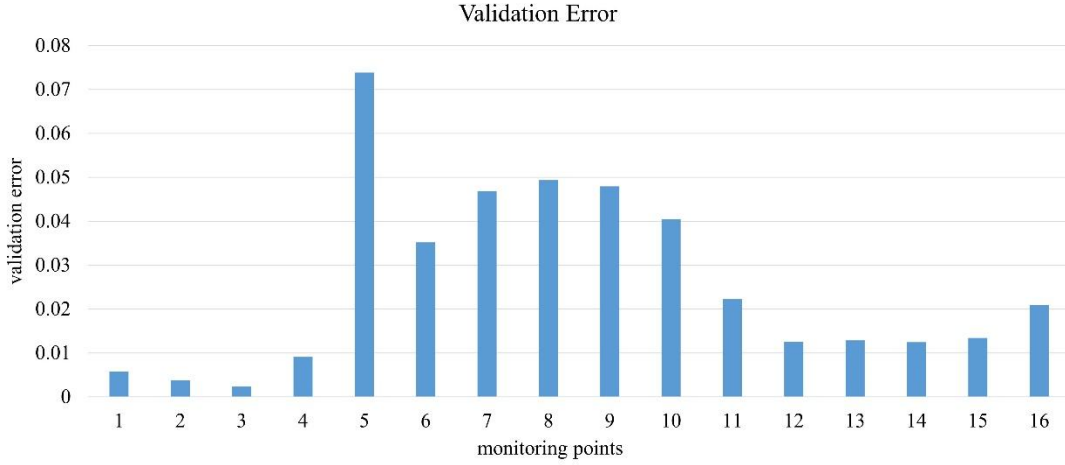


**Figure 5. Validation error according to the 16 monitoring points**

### 5.1.2 Model Inadequacy

Not only description of the uncertainty related with the model coefficients, but description of the uncertainty from model is also important. Because the turbulent models, especially RANS, are derived from the assumption of relatively simple flows like isotropic turbulence and boundary layer flow, they are different from the actual turbulence phenomenon in complex flow. This model inadequacy becomes a source of uncertainty that propagates through the computational model and leads to errors in the prediction of the model. Assuming  $\tilde{\mathbf{d}}$  as the true process with no error, then the computational model  $\mathcal{M}(\mathbf{X})$  and the model inadequacy  $\eta$  can be related as follows:

$$\tilde{\mathbf{d}} = \mathcal{M}(\mathbf{X}) + \eta \quad (5.3)$$

Cheung et al. [3] suggested a three-model classification of model inadequacy (no uncertainty, independent Gaussian uncertainty, and correlated Gaussian uncertainty). The correlated Gaussian uncertainty showed the highest posterior plausibility among these model classes.

$$\eta \sim \text{Gaussian}(0, K_\eta), \quad K_\eta = \sigma_\eta^2 \exp \left[ -\frac{1}{2} \left( \frac{x - x'}{l} \right)^2 \right] \quad (5.4)$$

$$\sigma_\eta \sim \text{Uniform}(0, 0.1) \quad (5.5)$$

Those researchers only considered the model error variation with one kind of covariance function. Therefore, the present work considers three kinds of covariance functions (Linear, Gaussian, and Matérn 5/2) as follows:

$$K_\eta = \sigma_\eta^2 \max \left( 0, 1 - \frac{|x - x'|}{l} \right) \quad (5.6)$$

$$K_\eta = \sigma_\eta^2 \exp \left[ -\frac{1}{2} \left( \frac{x - x'}{l} \right)^2 \right] \quad (5.7)$$

$$K_{\eta} = \sigma_{\eta}^2 \left( 1 + \frac{\sqrt{5}|x - x'|}{l} + \frac{5}{3} \frac{|x - x'|^2}{l^2} \right) \exp \left[ -\frac{\sqrt{5}|x - x'|}{l} \right] \quad (5.8)$$

where  $\sigma_{\eta}$  is the variance magnitude and  $l$  is the characteristic length. The correlation metrics according to distance are shown in Fig. 6. In the order of Linear, Matérn 5/2, and Gaussian covariance functions, the correlation according to the distance was less expressed. This means that the Linear covariance function can be used for models where the uncertainty propagation does not spread far, and the Gaussian function can be applied in the opposite case.

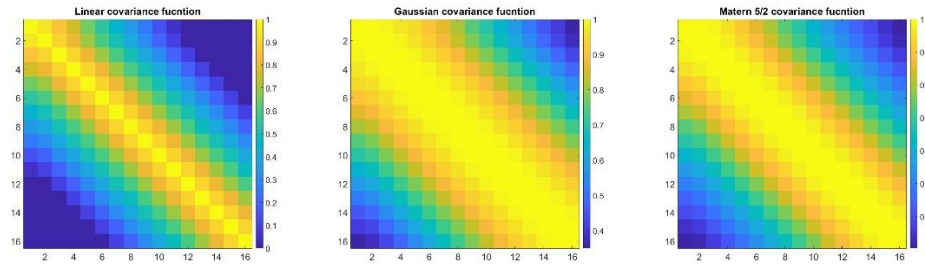


**Figure 6. Correlation metrics for each covariance function**

### 5.1.3 Observation Error

Observation error is one of the unavoidable uncertainties in experimental works. parameter uncertainty is calibrated by experimental data, modeling the observation error is important process in Bayesian inference. However, information on the error bars of the experimental data [5] could not be obtained, it was assumed to be an independent Gaussian model. The true process  $\tilde{\mathbf{d}}$ , observation error  $\mathbf{e}$ , and observation data  $\mathbf{d}$  can be related as follows:



$$\mathbf{d} = \tilde{\mathbf{d}} + \mathbf{e} \quad (5.9)$$

$$\mathbf{e} \sim \text{Gaussian}(0, K_e), \quad K_e = \sigma_e^2 I \quad (5.10)$$

$$\sigma_e \sim \text{Uniform}(0, 0.02) \quad (5.11)$$

where  $K_e$  is a diagonal matrix with each diagonal component equal to the variance. Observation errors are independent Gaussian random variables with zero mean and standard deviation.

## 5.2 Likelihood Function

All stochastic models are combined into the likelihood function. From Eqs. (5.3) and (5.9), observation data can be expressed by a conditional Gaussian distribution as follows:

$$\mathbf{d} | \boldsymbol{\sigma}, \mathbf{X} \sim \text{Gaussian}(\mathcal{M}(\mathbf{X}), K) \quad (5.12)$$

where  $\boldsymbol{\sigma}$  is the uncertainty parameter including  $\sigma_e$  and  $\sigma_\eta$ , and  $K$  is the covariance matrix that is the sum of  $K_\eta + K_e$ . Finally, if all the inferred uncertainty parameters ( $\boldsymbol{\sigma}, \mathbf{X}$ ) are put to  $\boldsymbol{\theta}$ , the likelihood function and posterior distribution can be expressed as follows:

$$P(\mathbf{d} | \boldsymbol{\theta}) = \frac{1}{Z} \frac{1}{\sqrt{(2\pi)^N \det(K)}} \exp\left(-\frac{1}{2}(\mathbf{d} - \mathcal{M}(\mathbf{X}))^T K^{-1}(\mathbf{d} - \mathcal{M}(\mathbf{X}))\right) \quad (5.13)$$

$$Z = \int P(\mathbf{d}|\boldsymbol{\theta})P(\boldsymbol{\theta})d\boldsymbol{\theta} \quad (5.14)$$

$$P(\boldsymbol{\theta}|\mathbf{d}) = \frac{1}{Z} \frac{1}{\sqrt{(2\pi)^N \det(K)}} \exp\left(-\frac{1}{2}(\mathbf{d} - \mathcal{M}(\mathbf{X}))^T K^{-1}(\mathbf{d} - \mathcal{M}(\mathbf{X}))\right) P(\boldsymbol{\theta}) \quad (5.15)$$

### 5.3 Markov Chain Monte Carlo (MCMC)

In practice, posterior distributions do not have a closed-form solution. One widely-used option to solve inverse problems relies upon MCMC [14]. The basic idea of MCMC simulations is to construct a Markov chain that equals the posterior distribution over the prior support  $\mathcal{D}_X$ . Markov chains can be uniquely defined by their transition probability  $\mathcal{K}(x^{(t+1)}|x^{(t)})$  from the step  $x^{(t)}$  of the chain at iteration  $t$  to the step  $x^{(t+1)}$  at the subsequent iteration  $t + 1$ . Then, the posterior is equal to the Markov chain if the specified transition probability fulfils the detailed balance condition:

$$\pi(x^{(t)}|y) \mathcal{K}(x^{(t+1)}|x^{(t)}) = \pi(x^{(t+1)}|y) \mathcal{K}(x^{(t)}|x^{(t+1)}) \quad (5.16)$$

One of the algorithms to fulfill this equation is the Metropolis-Hastings (MH) algorithm [15] that is based on proposing and subsequently accepting or rejecting candidate points. At iteration  $t$  from the current sample  $x^{(t)}$ , one then draws a candidate sample  $x^{(*)}$  from a proposal distribution  $p(x^{(*)}|x^{(t)})$ . Subsequently, the candidate is accepted with a probability as follows:

$$\alpha(x^{(*)}, x^{(t)}) = \min\left\{1, \frac{\pi(x^{(*)}|y)p(x^{(t)}|x^{(*)})}{\pi(x^{(t)}|y)p(x^{(*)}|x^{(t)})}\right\} \quad (5.17)$$

However, most MCMC algorithms perform poorly when the target distribution shows strong correlations between the parameters. A considerable amount of tuning is necessary to improve the performance of these algorithms. The affine invariant ensemble (AIES) algorithm [16] alleviates this problem to being invariant with affine transformation of the target distribution. The affine invariance property is achieved by generating proposals according to a so-called stretch move. This refers to proposing a new candidate by:

$$x_i^{(*)} = x_i^{(t)} + Z(x_j^{(t)} - x_i^{(t)}), \text{ where } Z \sim p(z) = \begin{cases} \frac{1}{\sqrt{z}(2\sqrt{a} - \frac{2}{\sqrt{a}})} & \text{if } z \in [\frac{1}{a}, a] \\ 0 & \text{otherwise} \end{cases} \quad (5.18)$$

This requires sampling from the distribution  $p(z)$  defined by the tuning parameter  $a > 1$ . The candidate  $x_i^{(*)}$  is then accepted as the new location of the  $i$ -th walker with a probability as follows:

$$\alpha(x_i^{(*)}, x_i^{(t)}, z) = \min \left\{ 1, z^{M-1} \frac{\pi(x_i^{(*)} | \mathbf{y})}{\pi(x_i^{(t)} | \mathbf{y})} \right\} \quad (5.19)$$

In the present work, AIES was applied to sampling the posterior distribution with 2000 steps and 300 parallel chains.

## 5.4 Posterior Distribution

### 5.4.1 Model Evidence

Cheung et al [3,17] applied Bayesian methodology to find the best stochastic model for the given data. This study also used model evidence to find best stochastic model. And

found the maximum likelihood from the posterior samples of each stochastic model and compared them in terms of model evidence.  $M_2$ (Gaussian covariance) was most favored over the other two model classes as shown in Table 5. As mentioned at 5.1.2, Gaussian covariance showed a wide spread of the correlation, and this characteristic of  $M_2$  represented the best spatial correlation in the given data.

**Table 5. Posterior plausibility of the model classes**

Stochastic Model	Posterior Plausibility
$M_1$ (Linear covariance)	0.1805
$M_2$ (Gaussian covariance)	0.4973
$M_3$ (Matérn 5/2 covariance)	0.3222

### 5.4.2 Posterior Results

From the results of the posterior plausibility, all posterior results were calculated through the Gaussian covariance. Figures 7-10 show the posterior distributions for the four model coefficients of the Transition SST model ( $c_{a1}, c_{e1}, c_{a2}, c_{e2}$ ) with  $\pm 10\%$  intervals from each nominal value. Most of the posterior distributions are truncated at the boundary of the uncertainty range. This means that the estimated model coefficients were outside the prior setup, so the prior range was extended by  $\pm 50\%$  from each nominal value.

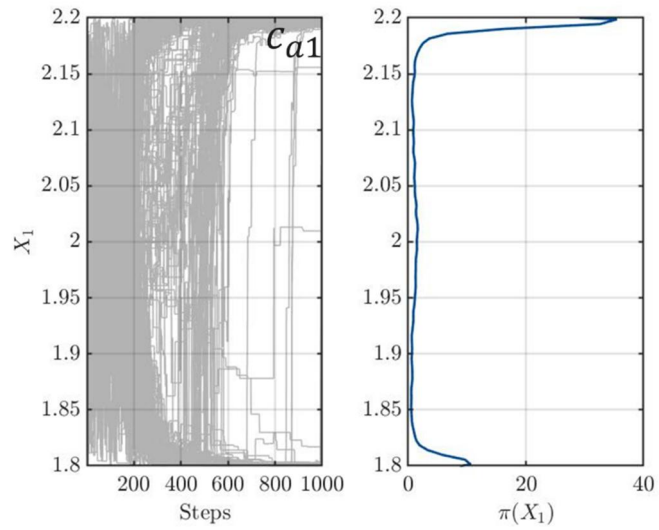


**Figure 7. Posterior distribution for  $\pm 10\%$  interval  $c_{a1}$**

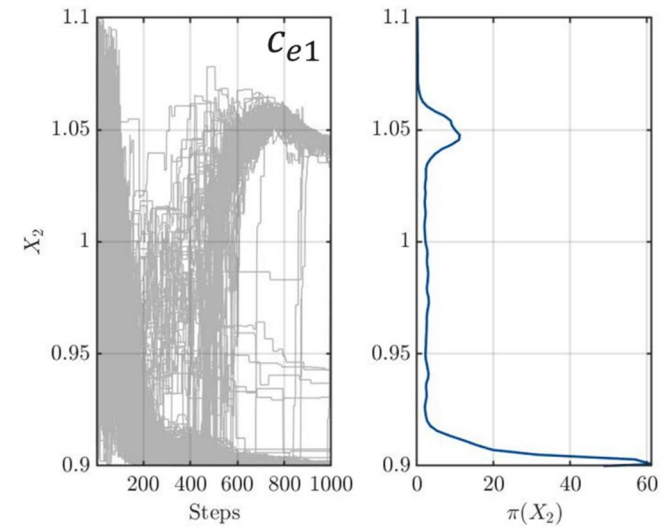


**Figure 8. Posterior distribution for  $\pm 10\%$  interval  $c_{e1}$**

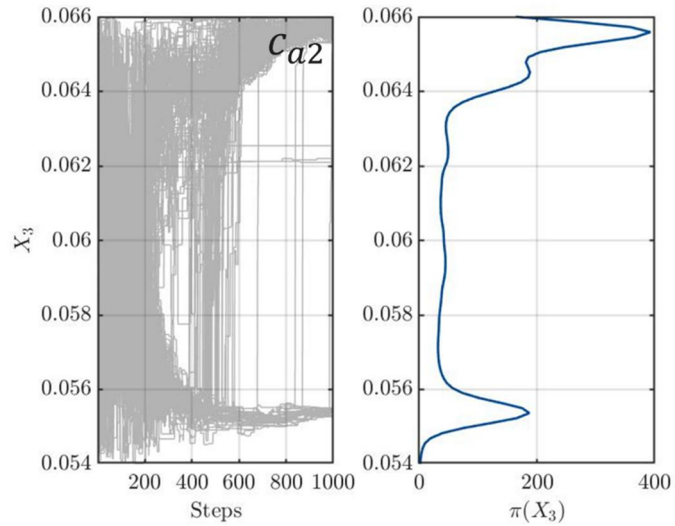


**Figure 9. Posterior distribution for  $\pm 10\%$  interval  $c_{a2}$**

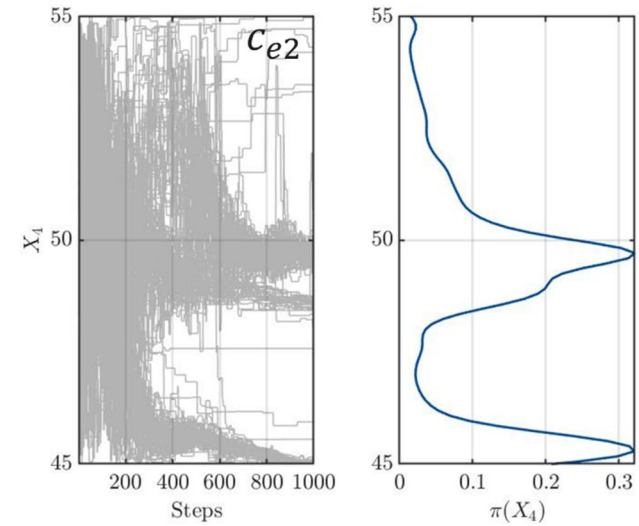


**Figure 10. Posterior distribution for  $\pm 10\%$  interval  $c_{e2}$**

Figures 11-17 show the posterior distributions for the seven model coefficients of the Transition SST model ( $c_{a1}, c_{e1}, c_{a2}, c_{e2}, \sigma_\gamma, c_{\theta t}$  and  $\sigma_{\theta t}$ ) with  $\pm 50\%$  intervals from each nominal value. The noticeable changes in the posterior distributions are the  $c_{a1}, c_{e1}$ , which were known as the major model coefficients from a previous study by Bae and Chang [18]. The model coefficient  $c_{a1}$  (located in the intermittency product term, and it controls the transition region with  $F_{length}$ ) increased and  $c_{e1}$  (opposite to  $c_{a1}$ ) decreased from the nominal value. When comparing the experiment results with the simulation results of the nominal values, these changes were natural because the simulation predicted a longer transition region. This means that these changes reflected the experimental results through the Bayesian inference. Figures 18 and 19 show the posterior distributions for the uncertainty parameters ( $\sigma_\eta, \sigma_e$ ). They indicate that uncertainty from the model inadequacy had a standard deviation of 2% of the Transition SST model  $C_f$  prediction. In contrast, the observation error was estimated to be negligible with a standard deviation of 0.2%.

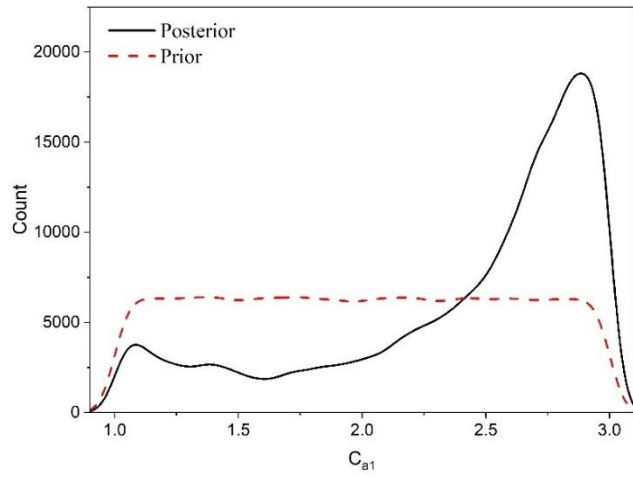


Figure 11. Posterior distribution for  $\pm 50\%$  interval  $c_{a1}$

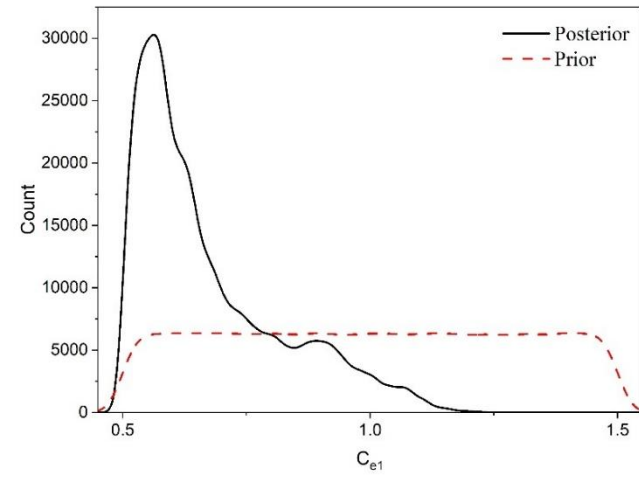


Figure 12. Posterior distribution for  $\pm 50\%$  interval  $c_{e1}$

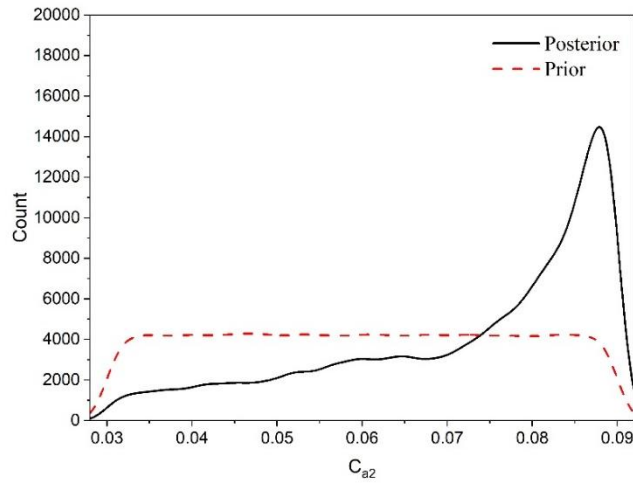


Figure 13. Posterior distribution for  $\pm 50\%$  interval  $c_{a2}$

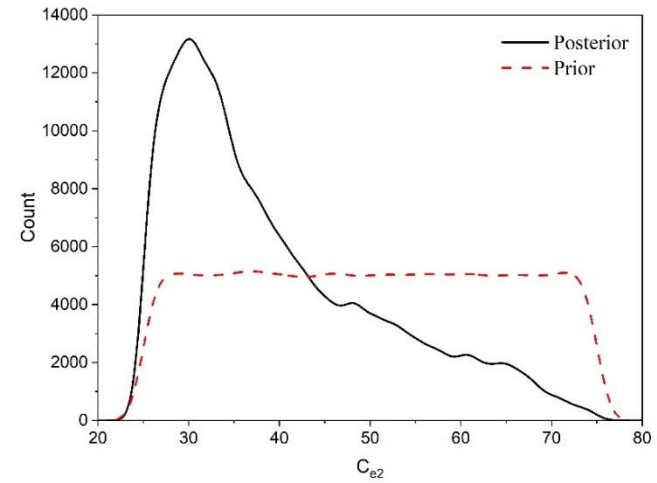
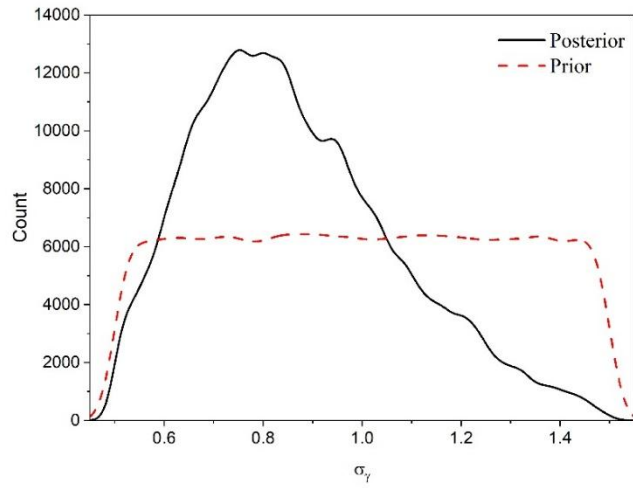
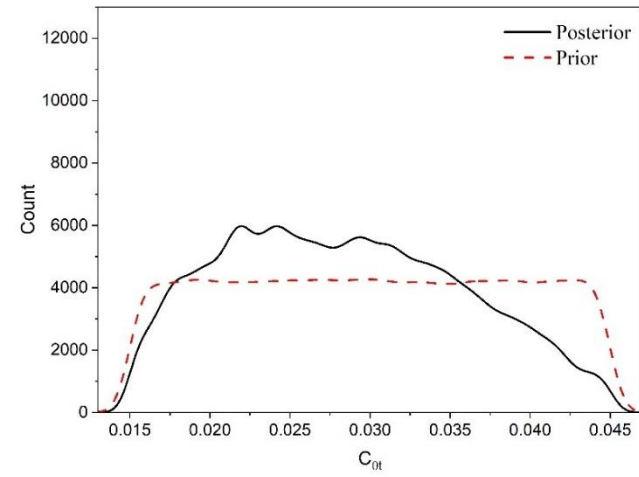


Figure 14. Posterior distribution for  $\pm 50\%$  interval  $c_{e2}$



**Figure 15. Posterior distribution for  $\pm 50\%$  interval  $\sigma_\gamma$**



**Figure 16. Posterior distribution for  $\pm 50\%$  interval  $c_{\theta t}$**

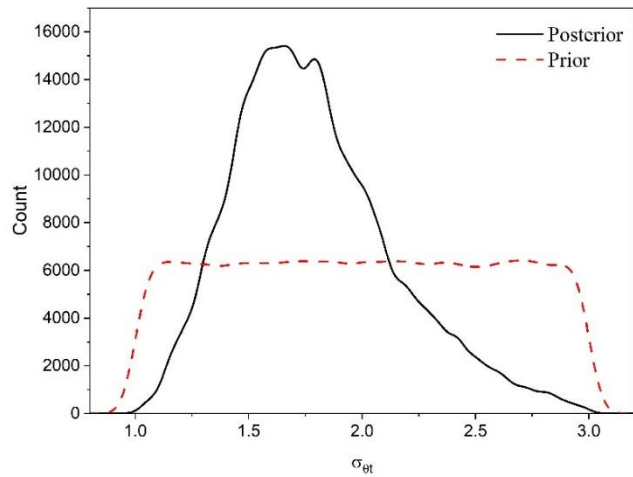


**Figure 17. Posterior distribution for  $\pm 50\%$  interval  $\sigma_{\theta t}$**



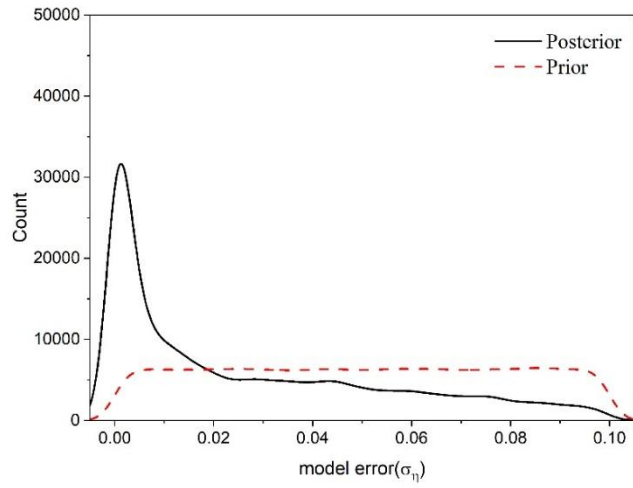


**Figure 18. Posterior distribution for  $\sigma_\eta$**

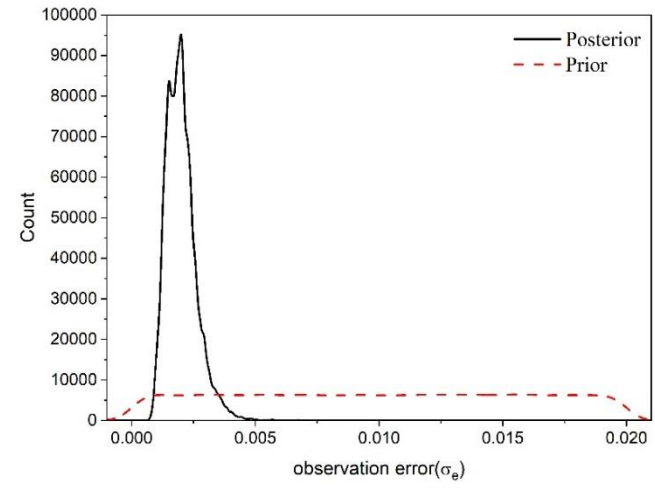


**Figure 19. Posterior distribution for  $\sigma_e$**

Table 6 shows the calibrated model coefficients from the posterior distribution mean, and Figs. 20 and 21 show the  $C_f$  predictions using the calibrated model coefficients. As mentioned above, comparing the experimental results with the simulation results of the nominal values, it predicted a longer transition region, but the calibrated value predicted a transition region shorter than the nominal one and the  $C_f$  prediction was improved by up to 6% in the transition region.

**Table 6. Calibrated Transition SST model closure coefficients**

Model Coefficient	Nominal Value	Calibrated Value
$c_{a1}$	2.0	2.4
$c_{e1}$	1.0	0.67
$c_{a2}$	0.06	0.072
$c_{e2}$	50.0	39.0
$\sigma_\gamma$	1.0	0.87
$c_{\theta t}$	0.03	0.028
$\sigma_{\theta t}$	2.0	1.8

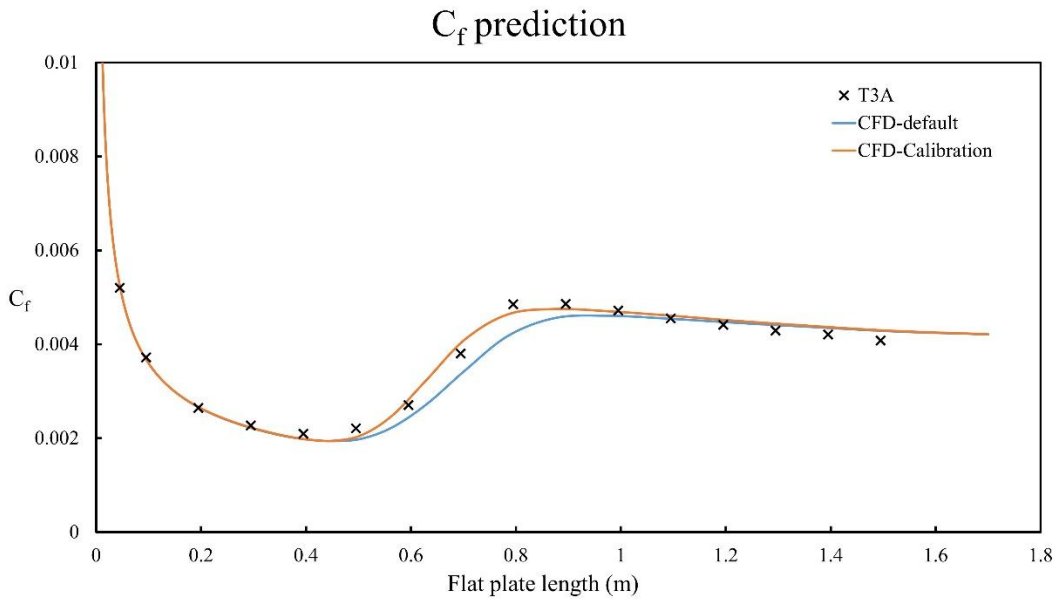


Figure 20.  $C_f$  predictions using calibrated model coefficients

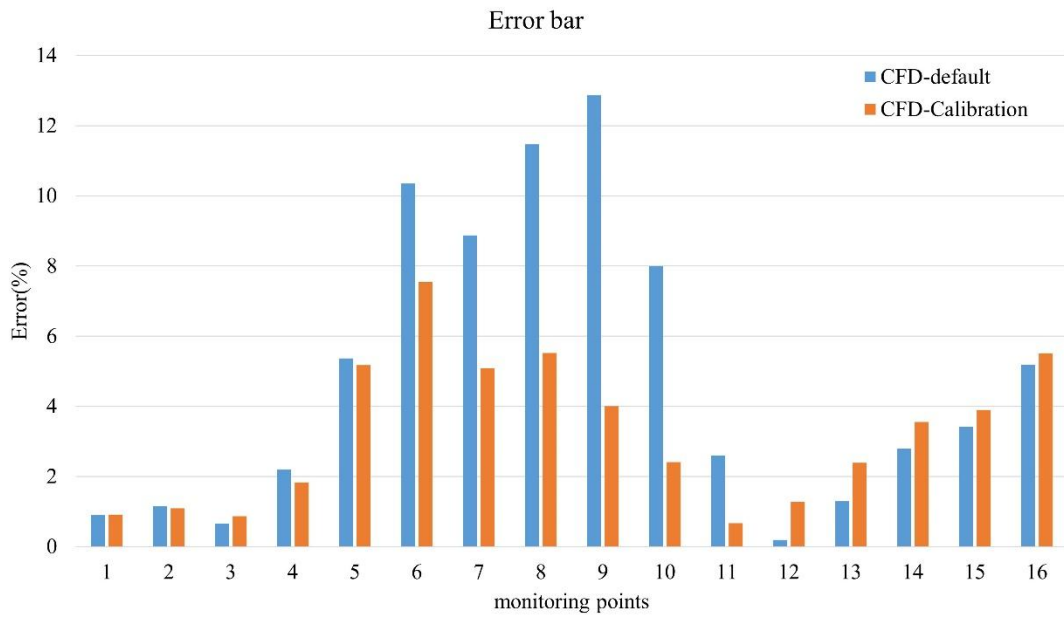


Figure 21.  $C_f$  prediction errors compared with nominal values

## Chapter 6. Conclusion

In the present work, Transition SST model coefficients and uncertainty are calibrated and quantified through the Bayesian inference using experimental data (T3A [5]). For the experimental data, the skin friction coefficient of the zero-pressure gradient transition flow around a flat plate was used, and then a 2D flat plate CFD simulation was conducted under similar flow conditions.

Three kinds of uncertainty in the computational model are considered. Uncertainty from the model coefficients was modeled with independent uniform distributions within  $\pm 10\%$  and  $\pm 50\%$  intervals from each nominal value. It was then calculated by an NIPC expansion-based surrogate model instead of the 2D flat plate CFD simulation. Uncertainty from model inadequacy was modeled with a correlated additive Gaussian model [3] with three kinds of covariance functions, although uncertainty from the observation errors was modeled with an independent additive Gaussian model because information on error bars could not be obtained. AIES was used for posterior distribution sampling: a total of 600,000 samples were used in 2,000 steps and 300 parallel chains.

In the results, the major variables  $c_{a1}$  and  $c_{e1}$  increased and decreased, respectively, and these changes made the transition region shorter than the nominal one; this seemed to be the result of Bayesian inference reflecting the experimental data. The posterior results pertaining to model inadequacy and observation error indicated a standard deviation of 2% in the Transition SST model  $C_f$  prediction, and a standard deviation of 0.2% in the experimental data. The Transition SST model using calibrated model coefficients predicted a transition region shorter than the nominal one, and the  $C_f$  prediction was improved by up to 6% in the transition region.

## REFERENCES

1. Hosder, S., Walters, R., Perez, R., 2006. A non-intrusive polynomial chaos method for uncertainty propagation in CFD simulations. In 44th AIAA aerospace sciences meeting and exhibit, pp.891.
2. Schaefer, J., Hosder, S., West, T., Rumsey, C., Carlson, J. R., Kleb, W., 2017. Uncertainty quantification of turbulence model closure coefficients for transonic wall-bounded flows. *AIAA Journal*, 55(1), pp.195-213.
3. Cheung, S. H., Oliver, T. A., Prudencio, E. E., Prudhomme, S., Moser, R. D., 2011. Bayesian uncertainty analysis with applications to turbulence modeling. *Reliability Engineering & System Safety*, 96(9), pp.1137-1149.
4. Zhang, J., Fu, S., 2018. An efficient Bayesian uncertainty quantification approach with application to  $k-\omega-\gamma$  transition modeling. *Computers & Fluids*, 161, pp.211-224.
5. Coupland, J., 1990. Ercoftac special interest group on laminar to turbulent transition and retransition: T3a and t3b test cases. A309514.
6. Langtry, R. B., Menter, F. R., 2009. Correlation-based transition modeling for unstructured parallelized computational fluid dynamics codes. *AIAA Journal*, 47(12), pp.2894-2906.
7. Van Doormaal, J. P., Raithby, G. D., 1984. Enhancements of the SIMPLE method for predicting incompressible fluid flows. *Numerical heat transfer*, 7(2), pp.147-163.
8. Malan, P., Suluksna, K., Juntasaro, E., 2009. Calibrating the gamma-Re\_theta transition model for commercial CFD. In 47th AIAA Aerospace Sciences Meeting Including The New Horizons Forum and Aerospace Exposition, pp.1142.
9. Kennedy, M. C., O'Hagan, A., 2001. Bayesian calibration of computer models. *Journal of the Royal Statistical Society: Series B (Statistical Methodology)*, 63(3), pp.425-464.
10. S. Marelli., B. Sudret., 2014. UQLab: A framework for uncertainty quantification in Matlab, Proc. 2nd Int. Conf. on Vulnerability, Risk Analysis and Management

(ICVRAM2014), Liverpool, United Kingdom, 2554-2563

11. MATLAB, The MathWorks, Inc., Release 2020b
12. Hosder, S., Walters, R. W., 2007. Non-intrusive polynomial chaos methods for stochastic CFD-theory and applications. In RTO Meeting Proceedings. Computational Uncertainty in Military Vehicle Design.
13. S. Marelli., B. Sudret., 2019. UQLab user manual – Polynomial chaos expansions, Report # UQLab-V1.3-104, Chair of Risk, Safety and Uncertainty Quantification, ETH Zurich, Switzerland.
14. P.R. Wagner., J. Nagel., S. Marelli., B. Sudret., 2019. UQLab user manual – Bayesian inference for model calibration and inverse problems, Report # UQLab-V1.3-113, Chair of Risk, Safety and Uncertainty Quantification, ETH Zurich, Switzerland.
15. Hastings, W. K., 1970. Monte Carlo sampling methods using Markov chains and their applications.
16. Goodman, J., Weare, J., 2010. Ensemble samplers with affine invariance. *Communications in applied mathematics and computational science*, 5(1), pp.65-80.
17. Cheung, S. H., Beck, J. L., 2010. Calculation of posterior probabilities for Bayesian model class assessment and averaging from posterior samples based on dynamic system data. *Computer-Aided Civil and Infrastructure Engineering*, 25(5), pp.304-321.
18. J.H. Bae., K. Chang., 2021. Bayesian Inference for Transition Model Coefficients based on Zero-pressure Gradient Experimental Data. *Transaction of the Korean Society of Mechanical Engineers B*, 45(12), pp. 655~662.